Nucleic Acids Research, 2023, **51**, 11706–11716
https://doi.org/10.1093/nar/gkad850
Advance access publication date: 18 October 2023
Genome integrity, repair and replication

The SAP domain of Ku facilitates its efficient loading onto DNA ends

Jaroslav Fulneček[1], Eva Klimentová[1], Albert Cairo[1], Sona Valuchova Bukovcakova[1], Panagiotis Alexiou[1], Zbynek Prokop[2,3] and Karel Riha[1,*]

[1]CEITEC Masaryk University, Brno, Czech Republic
[2]Loschmidt Laboratories, Department of Experimental Biology and RECETOX, Masaryk University, Brno, Czech Republic
[3]International Clinical Research Center, St Anne's University Hospital, Brno, Czech Republic

*To whom correspondence should be addressed. Tel: +420 549 49 7836; Email: karel.riha@ceitec.muni.cz
Present address: Panagiotis Alexiou, Faculty of Health Sciences, University of Malta, Msida, Malta.

Abstract

The evolutionarily conserved DNA repair complex Ku serves as the primary sensor of free DNA ends in eukaryotic cells. Its rapid association with DNA ends is crucial for several cellular processes, including non-homologous end joining (NHEJ) DNA repair and telomere protection. In this study, we conducted a transient kinetic analysis to investigate the impact of the SAP domain on individual phases of the Ku–DNA interaction. Specifically, we examined the initial binding, the subsequent docking of Ku onto DNA, and sliding of Ku along DNA. Our findings revealed that the C-terminal SAP domain of Ku70 facilitates the initial phases of the Ku–DNA interaction but does not affect the sliding process. This suggests that the SAP domain may either establish the first interactions with DNA, or stabilize these initial interactions during loading. To assess the biological role of the SAP domain, we generated Arabidopsis plants expressing Ku lacking the SAP domain. Intriguingly, despite the decreased efficiency of the ΔSAP Ku complex in loading onto DNA, the mutant plants exhibited full proficiency in classical NHEJ and telomere maintenance. This indicates that the speed with which Ku loads onto telomeres or DNA double-strand breaks is not the decisive factor in stabilizing these DNA structures.

Graphical abstract

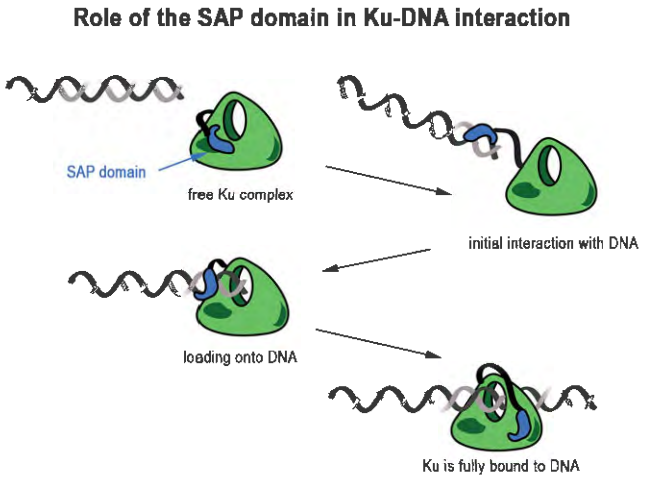

Introduction

The DNA repair complex known as Ku plays a central role in maintaining genome integrity. Ku is composed of two subunits, Ku70 and Ku80, which form a heterodimer that binds to DNA ends. It acts as an initial responder to DNA damage, rapidly recognizing and binding to DNA double-strand breaks (DSBs) (1,2). Once bound, Ku stabilizes DSBs by preventing their degradation and recruits and activates other DNA repair proteins, initiating a cascade of DNA damage signaling and processing events that culminate in the rejoining of broken DNA ends. This DNA repair mechanism is known as non-homologous end joining (NHEJ) and represents the major DSB repair pathway in the G1/G0 phase of the cell cycle. Ku is evolutionarily conserved across all eukaryotes and is the defining component of NHEJ. When NHEJ is impaired, DSBs can be repaired by alternative end-joining pathways (alt-EJ)

Received: June 26, 2023. **Revised:** September 11, 2023. **Editorial Decision:** September 14, 2023. **Accepted:** September 29, 2023

that may result in more extensive resection of DNA ends, and their lower accuracy increases the risk of chromosomal rearrangements (3).

In addition to its role in NHEJ, Ku has also been implicated in other aspects of DNA end metabolism including detection of DNA viruses (4), V(D)J recombination, and stabilization and restart of arrested replication forks (5,6). Furthermore, Ku is important for maintenance and protection of telomeres, specialized chromatin structures that shield natural ends of linear eukaryotic chromosomes from being recognized as DSBs (7,8). Ku-deficient mutants often exhibit chromosome end deprotection characterized by nucleolytic resection of telomeres, increased recombination, and chromosome fusions. The involvement of Ku at telomeres is seemingly contra-intuitive, because one of the key hallmarks of telomere dysfunction, chromosome end-to-end fusions, is mediated by NHEJ. Thus, it is assumed that Ku activity is modulated in the context of telomeres to assure end protection while preventing downstream steps of NHEJ.

These diverse functions of Ku are implemented through its binding to free DNA ends. Ku exhibits a strong sequence-independent affinity to DNA ends and is assumed to be the major DNA-end binding factor in eukaryotic cells (8). The affinity to DNA ends stems from the structural properties of the Ku heterodimer. The Ku70 and Ku80 proteins share a similar topology, consisting of an N-terminal α/β domain, a central antiparallel β-barrel and C-termini composed of a subunit-specific globular domain connected with the protein core by a flexible linker. The Ku heterodimer forms a ring-like structure with a positively charged channel through which DNA is threaded, resembling a nut and bolt mechanism. (9). Ku is loaded onto DNA directionally, with the Ku80 side of the heterodimer oriented towards the DNA end (10). Mutations altering the electrostatic charge in the leading part of the channel abolish the Ku–DNA interaction (11,12), validating the essential role of the channel in DNA binding. Once loaded onto DNA, Ku can freely slide along duplex DNA using an energy-free mechanism that is not fully understood.

Another portion of Ku implicated in DNA interaction is the C-terminal region of Ku70, which includes a flexible loop and the SAP (SAF-A/B, Acinus and PIAS) domain. The SAP domain was identified through a bioinformatic search as a putative DNA binding motif that is enriched in proteins involved in chromosomal organization, DNA repair, and transcription (13). The Ku70 SAP domain adopts a unique helix-extended loop-helix structure with patches of positively charged residues on its surface, suggesting potential interaction with DNA (9,14,15). Indeed, the SAP domain has been reported to interact with DNA, although at a much lower affinity than the Ku70/80 central channel, and deletions spanning the Ku70 C-terminus have been shown to impair Ku–DNA binding *in vitro* (14,16,17). Cryo-EM studies indicate that the SAP domain does not assume a fixed position in the complex but undergoes a change in its location upon DNA binding (18,19). Interestingly, the SAP domain in the DNA-bound Ku complex is positioned distally from the central channel and does not directly contact DNA, raising the question of how SAP contributes to DNA binding. Furthermore, the contribution of the SAP domain to DNA repair and genome stability has not yet been assessed. Thus, the precise role of the SAP domain in the Ku–DNA interaction and its biological functions remain unknown.

While plants lack DNA-PKcs, they possess the core NHEJ proteins including the Ku complex, suggesting that the mechanism of plant NHEJ is analogous to that in yeast (20). Ku is dispensable in Arabidopsis and *ku* mutants do not exhibit any discernable growth or developmental defects, apart from an increased sensitivity to genotoxic stress (21–23). Inactivation of Ku also leads to partial telomere deprotection characterized by telomerase-mediated telomere extension, exonucleolytic resection of chromosome ends, and increased telomeric recombination (24–26). Protection of Arabidopsis telomeres is mediated by the physical association of Ku with chromosome termini through the central DNA binding channel, which parallels its association in the context of DSBs (12). However, mechanisms important for Ku–DNA binding differ at telomeres and in NHEJ. Mutations in the central channel of the Ku complex, which impair its translocation along DNA, retain telomere protection but result in deficient DNA repair (12). These observations suggest that, in the context of a DSB, Ku translocation is required to free the end for downstream processing and ligation, while entrapment of Ku at chromosome termini is sufficient for telomere protection.

The ability to functionally distinguish the Ku–DNA binding requirements in two biological processes prompted us to examine the role of the Ku70 SAP domain in Arabidopsis. In this study, we analyzed the role of the SAP domain on kinetics of the Ku–DNA interaction *in vitro*, and examined the contribution of the SAP domain to c-NHEJ and telomere maintenance *in vivo*.

Materials and methods

Plant material

The *Arabidopsis thaliana* ecotype Col-0 *ku70-2* line (SALK_123114) with a T-DNA insertion in the N-terminal region of the *KU70* gene (12). Complementation vectors and transgenic plants At18 and At25 were previously described (12). Plants were grown in phytotrons under LED illumination (white 77% /red 20% /infrared 3%; 150 μmol m-2 s -1) with 16/8 h light/dark regime. Genotyping was carried out by PCR with primers indicated in Supplementary Table S1.

Plant transformation

The plant binary vector for producing ΔSAP plants was derived from pCBSV70wt, which encodes the full-length Ku70 (12), by deleting nucleotides coding for L593-K621 using an *in vitro* mutagenesis based method (27) with primers listed in Supplementary Table S1. Binary vectors were electroporated into *Agrobacterium tumefaciens* GV3101 and Arabidopsis plants heterozygous for *ku70-2* were transformed by the floral dip method. Transformed plants were selected on soil sprayed with 40 μg/ml BASTA. *ku70* mutants homozygous for the transgene were used for analysis. Protein levels in transgenic plants were examined by immunoblotting using rabbit anti AtKu70 (12) and detected on LiCor Odyssey using goat IRDye 800 CW α- rabbit (LI-COR Biosciences).

Telomere analyses

Terminal restriction fragment analysis and t-circle amplification were performed as previously described (24,26).

Genotoxicity assays

Arabidopsis seeds were surface sterilized by Cl_2 evaporation, and approximately 50 seeds were put on 0.5× Murashige and

Skoog (MS) agar plates supplemented with bleomycin at the indicated concentrations (Calbiochem). Seeds were stratified at +4°C for two days and then incubated at 21°C in cultivation chambers (16/8 h light/dark cycle, light 60 μmol m^{-2} s^{-1}). Seedlings were scored 11 days after germination. Root growth assays were performed in a similar way in square plates positioned vertically in holders at an angle of 80°.

Protein expression and purification

The expression vector pFastBac Dual (Invitrogen) was used to co-express Arabidopsis Ku70 and His-tagged Ku80 subunits in insect cells using a baculovirus expression system at Vienna BioCenter Core Facility as described previously (12). The vector for production of ΔSAP Ku70 was generated by deleting nucleotides coding for L593-K621 from pFastBac Dual Atwt plasmid (12) using an *in vitro* mutagenesis-based method. Briefly, the pFastBac Dual-based plasmids were transposed to EMBacY bacmid in *Escherichia coli* and subsequently transfected to Sf9 cells for baculovirus generation. The cells were infected with virus and harvested 3 days post infection. Cells were resuspended in lysis buffer (50 mM Tris–Cl, 250 mM KCl, 10% v/v glycerol, 1 mM DTT, pH 8.0) supplemented with protease inhibitors (Roche) and frozen in liquid nitrogen. Thawed cells were spun and Ku was bound to His Mag Sepharose Ni (GE Healthcare). Beads were washed in Lysis buffer containing 50 mM imidazole and Ku was eluted in Lysis buffer with 250 mM imidazole. Proteins were filtered using Nanosep centrifugal columns (Pall) and stored on ice.

DNA binding assays

EMSA was performed as previously described (12). mwPIFE was measured in Pierce NeutrAvidin coated black 96well plates (#15117, Thermo Scientific) in duplicate according to a published protocol (28). PIFE was measured in 50 μl of total volume with one pmol of immobilized Cy-3 labeled dsDNA probes and 6 pmol of Ku complex. Cy3-labelled DNA probes were prepared by annealing synthetized DNA oligonucleotides in annealing buffer (10 mM Tris–Cl pH 7.5, 50 mM NaCl, 1 mM EDTA) by heating to 95°C for 1 min in ThermoMixer C (Eppendorf) and cooling down to room temperature. Oligonucleotides used for generating the probes are listed in Supplementary Table S1. Stop-flow PIFE was measured using a three-syringe SFM-300 device equipped with a microcuvette μFC 08 cell (8 μl) and combined with a manual monochromator spectrometer MOS-200 equipped with a Xe arc 19 lamp (BioLogic, France). The instrument was operated by a BioKine 32 v 4.63. We applied excitation light at 547 nm and detected emission using a 585/65 ET Bandpass filter (AHF Analysentechnik) in 1 ms intervals for 1 s and 10 ms intervals for 20 s. The measurements were performed in the following buffer (150 mM KCl, 35 mM Tris–Cl pH 8.15, 1 mM EDTA, 0.1 mM DTT, 3.893 mM imidazole and 5.156% glycerol). 250 nM protein solution (the first syringe) was premixed with buffer (the second syringe) in a ratio from 0:10 to 10:0 and the premix was then mixed with 25 nM DNA oligonucleotides and, in the case of the 75 bp probe, also with 250 nM NeutrAvidin (Thermo Scientific, the third syringe) in a 1:1 ratio. An average trace was composed of at least five traces and was used for analysis. The fluorescence traces were fitted to single or double exponentials using KinTek Global Kinetic Explorer version 5.2 (KinTek, USA) providing the observed rate constants and amplitudes of individual kinetic phases (29).

DNA end joining assay

We used a 3400 bp DNA fragment (Supplementary Figure S1) containing the *35S-EYFP* gene derived from pGWB442 as a substrate for the end joining assay. The fragment was cleaved from pUC19 by *Sma*I, purified through agarose gel electrophoresis using NucleoSpin Gel and PCR Cleanup (Macherey-Nagel), eluted in water, and concentrated in SpeedVac Concentrator SAVANT SPD 121P (Thermo Fisher Scientific). The fragment was transfected in Arabidopsis mesophyll protoplasts according to (30) as follows: protoplasts were isolated from leaves of 4-week-old Arabidopsis grown on soil in a growth chamber at 22°C under 12/12 h light/dark cycles. 20–30 leaves were cut using a razor blade and digested in 15 ml of digestion solution (1% cellulase Onozuka R10 (Duchefa), macerozyme R10 (Duchefa), 0.4 M mannitol, 20 mM KCl, 20 mM MES pH 5.7), first for 20 min in vacuum followed by 3 h in the dark at room temperature. Released protoplasts were filtered with a 70 μm mesh, washed twice with W5 medium (154 mM NaCl, 125 mM $CaCl_2$, 5 mM KCl, 2 mM MES pH 5.7), and stored on ice. For transfection, the protoplasts were resuspended in MMg solution (0.4 mM mannitol, 15 mM $MgCl_2$, 4 mM MES pH 5.7) at 3×10^5 cells/ml. 100 μl of protoplasts were mixed with 10 μg of linearized DNA in a 10 μl maximal volume, added to 110 μl of PEG solution (4 g PEG 4000, 2.5 ml mannitol 0.8 M, 1 ml CaCl2 1 M, 3 ml H_20) and incubated for 10 min in the dark at RT. 440 μl of W5 medium was added to the mixture and, after centrifugation at 700 g for 3 min, the protoplasts were resuspended and incubated in 1 ml of fresh W5 medium for 16 h in the dark at room temperature. Transfected protoplasts were imaged for YFP fluorescence using a Zeiss LSM780 confocal microscope (objective LCI Plan-Neofluar 63×/1.3 1mm Korr DIC M27) to assess transfection efficiency, which was between 20 to 34%. Next, the protoplasts were collected for DNA extraction. After centrifugation at 700 g for 3 min, the supernatant was discarded and the pellet was frozen at –20°C for further extraction with the DNeasy® Plant Mini Kit (Qiagen). Total DNA was eluted in 10 μl of water and concentration was measured using NanoDrop. Re-joined ends were amplified by 35 cycles of PCR from 0.8 μl template using Q5 High-Fidelity DNA Polymerase (New England Biolabs) and primers NOSprom-nested-F2 and TagRFP-nested-R2 (Supplementary Table S1) in 20 μl reaction volume. Five tubes of each amplicon were pooled and DNA purified using NucleoSpin Gel and PCR Clean-Up (Macherey-Nagel). DNA was eluted in 20 μl of Elution Buffer and concentration was measured using Qubit 3.0 fluorometer (Life Technologies).

Sequencing libraries were prepared using KAPA Hyper Prep kit (Roche), using 1000 ng of amplicon DNA according to the manufacturer's protocol. We omitted any fragmentation steps and size-selected final libraries with AmpureXP magnetic beads (Beckman Coulter). The library was not amplified in the final step of preparation. Libraries were sequenced using the Illumina NextSeq instrument in mid output 2 × 150 cycles paired-end mode.

Raw FASTQ files from sequencing were quality checked, adapters and low-quality reads were trimmed using Trim Galore (v0.6.7) (https://github.com/FelixKrueger/TrimGalore) and reads shorter than 20 nt were discarded. The

paired-end reads were merged with PEAR (v0.9.6) (31). The pre-processed reads were subsequently mapped to the custom reference sequence with STAR (v2.7.10a) (32). Mapped reads were additionally post-processed to be able to count and visualize the different insertion and deletion types around the breakpoint. The reads were filtered to gain only reads containing insertion or deletion and clustered based on their mapping profile in the reference. The final file with clustered reads was visualized in IGV (33). The pipeline used for the processing from sequenced reads to the generation of visualizations is available at https://github.com/evaklimentova/DSB_pipeline. At least 50% of individual clusters per sample were manually evaluated for position and the length of deletion and quantified.

Results

The Ku70 SAP domain is evolutionarily highly conserved. It is present in plants, animals, and fungi (Supplementary Figure S2), suggesting its origin at the root of eukaryotic life. The Arabidopsis SAP domain shares 38% similarity with human SAP and contains a nuclear localization signal in its N-proximal part (Figure 1A). The Ku structure has so far been experimentally resolved only in humans. Nevertheless, AlphaFold (34) prediction indicates that the Arabidopsis Ku heterodimer forms an asymmetric ring-like structure highly similar to the crystal structure of human Ku (Figure 1B) (9). The SAP domain of Arabidopsis Ku70 is linked to the core of the complex with a long flexible linker and the AphaFold predicted helix-extended loop-helix structure perfectly overlays with the NMR-solved structure of human SAP (Figure 1C) (14). Thus, Arabidopsis Ku appears to have a very similar topology and structure to human Ku.

To analyze the impact of the SAP domain on Ku–DNA binding, we generated an Arabidopsis ΔSAP complex lacking the helix-extended loop-helix motif, but retaining the putative nuclear localization signal, by heterologous expression in insect cells (Figures 1A and 2A). Native polyacrylamide gel electrophoresis demonstrated that the ΔSAP complex forms stable heterodimers (Figure 2B). The effect of the SAP domain on the Ku–DNA interaction was assessed by electrophoretic mobility shift assay (EMSA) with a DNA duplex probe that can accommodate up to four Ku complexes. Whereas wild type Ku readily formed complexes containing probe bound with four Ku molecules, higher order complexes form less efficiently with ΔSAP and products with four Ku molecules were not detected in the tested concentration range (Figure 2C). This result corroborates data with human Ku and indicates that the SAP domain contributes to DNA binding.

In our previous work, we proposed that the Ku–DNA association is a multistep process consisting of an initial interaction of a DNA end with the Ku channel, Ku docking onto DNA, and sliding of Ku along DNA (Figure 3A) (12). To study the contribution of the SAP domain to Ku–DNA binding more in detail, we used an assay based on protein induced fluorescence enhancement (mwPIFE) (35). In this assay, protein bound in the immediate vicinity of a DNA-attached Cy3 fluorophore enhances emitted fluorescence, which can be used to measure protein-DNA interactions. We used DNA probes immobilized through one end to NeutrAvidin-coated microwell plates via biotin, while the opposite end was available for Ku binding. We have previously determined that the minimal binding site for Arabidopsis Ku is 13 bp (12). Therefore, we used 13 and 15 bp probes with Cy3 attached to DNA termini to assess the initial Ku–DNA interaction (Figure 3B). A 30 bp probe with Cy3 positioned 15 bp from DNA ends was used to monitor DNA docking; in this setting, fluorescent enhancement should occur only when Ku is fully loaded onto DNA. Finally, Ku translocation along DNA was tested using a 55 bp probe with Cy3 placed 40 bp from the free terminus. All probes showed a decreased PIFE signal with ΔSAP compared to wild type Ku (Figure 3B). Nevertheless, the difference in the PIFE signal between wt and ΔSAP was much smaller with the 55 bp probe, indicating that Ku's ability to slide along DNA is less affected than the initial binding steps.

We next performed a kinetic analysis of Ku–DNA binding in a stopped-flow system by scoring PIFE at millisecond intervals upon mixing Ku with DNA probes. We used a similar set of oligonucleotide probes as in the steady state measurements, with the exception that the 55 bp probe was extended to 75 bp, one end was blocked with biotin-neutravidin interaction, and the Cy3 fluorophore was placed 60 bp from the free end. Both wild type and ΔSAP produced PIFE signals that increased with time, generating kinetic curves (Figures 3C and S3). The kinetic curves were measured for different protein/DNA molar ratios, and the concentration dependencies of the observed rates were used to calculate the kinetic constants related to the individual steps of the Ku–DNA interaction (Table 1, Supplementary Figure S3).

Ku's interaction with the 15 and 30 bp probes revealed two kinetic phases that reflect the fast initial interaction followed by a slower conformational rearrangement, the 'docking' of the complex. The third kinetic phase, corresponding to sliding, was monitored with the 75 bp probe. Deletion of the SAP domain substantially slowed the initial interaction and docking phases, but did not have a profound impact on sliding (Figure 3C, Table 1). Anisotropy measurements with the 30 bp probe confirmed the fast formation of the initial interaction complex in wild type, which was not observed with ΔSAP (Figure 3D, E). Together, these findings indicate that the SAP domain facilitates the initial Ku–DNA interaction, while playing a minimal role in the subsequent sliding phase.

Arabidopsis mutants lacking Ku are viable, but exhibit partial telomere deprotection and sensitivity to genotoxic agents (21,23). To assess the function of the SAP domain in DNA repair and telomere protection, we complemented transgenic Arabidopsis plants with a disruption in the endogenous *KU70* gene with *KU70* constructs either with or without the SAP domain. Western blot analysis of several independent transgenic lines showed that the expression level of the Ku70 ΔSAP variant was substantially lower than the wild type Ku70 (Supplementary Figure S4). The lower level of Ku70 ΔSAP does not appear to be caused by proteasome-mediated degradation and rather indicates less efficient protein expression (Supplementary Figure S4C).

Arabidopsis *ku70* and *ku80* mutants have long telomeres due to unregulated extension by telomerase (25,36). Terminal restriction fragment analysis revealed that telomeres in *ΔSAP* plants were 3–6 kb, which is within the range of plants containing wild type Ku, whereas telomeres in Ku-deficient plants were over 10 kb (Figure 4A). Another characteristic of telomere deprotection in *ku70* mutants is increased telomeric recombination, leading to the formation of extrachromosomal telomeric circular DNA molecules (t-circles) (26). The telomeric circle amplification assay showed that the level of t-circles in *ΔSAP* plants is comparable to wild type (Figure 4B). This

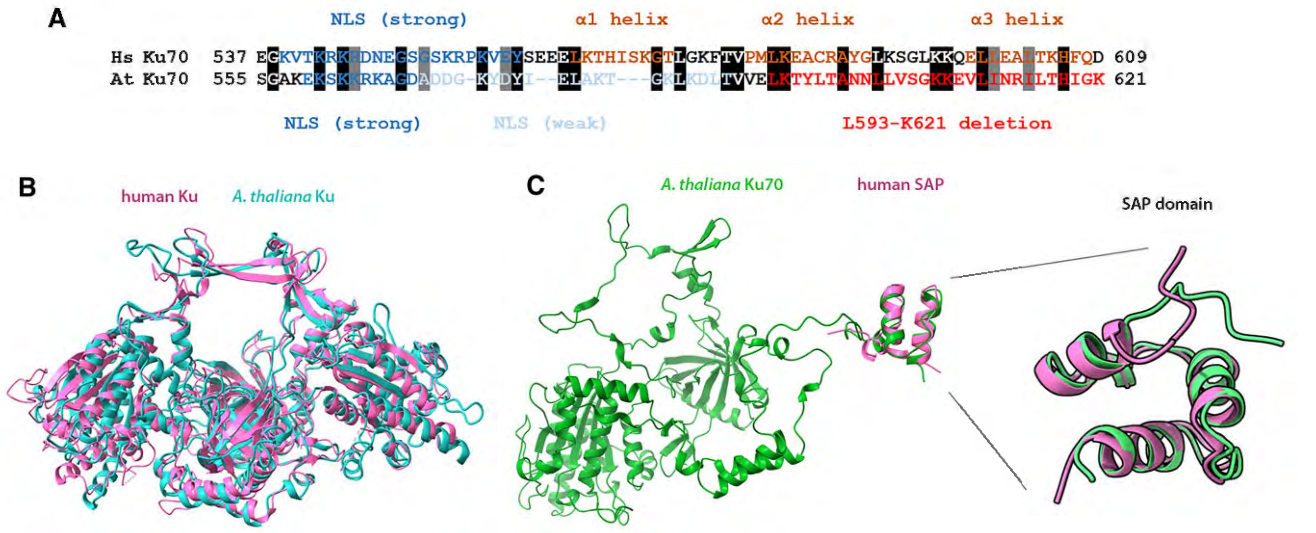

Figure 1. Structure of Arabidopsis Ku. (**A**) Sequence alignment of human (Hs) and *Arabidopsis thaliana* (At) Ku70 c-terminal region depicted with predicted nuclear localization signals (NLS), alpha helices, and the region deleted in the *ΔSAP* variant. (**B**) Superimposed structures of human Ku obtained by X-ray crystallography (1JEQ; violet) and Arabidopsis Ku predicted by AlphaFold (cyan) to show the similarity of the core complexes (without Ku80 and Ku70 C-termini). (**C**) Structure of Arabidopsis Ku70 predicted by AlphaFold including the SAP domain and the flexible linker. The structure of the human SAP domain determined by NMR (1JJR; violet) is superimposed over the Arabidopsis SAP domain (green) using ChimeraX (45).

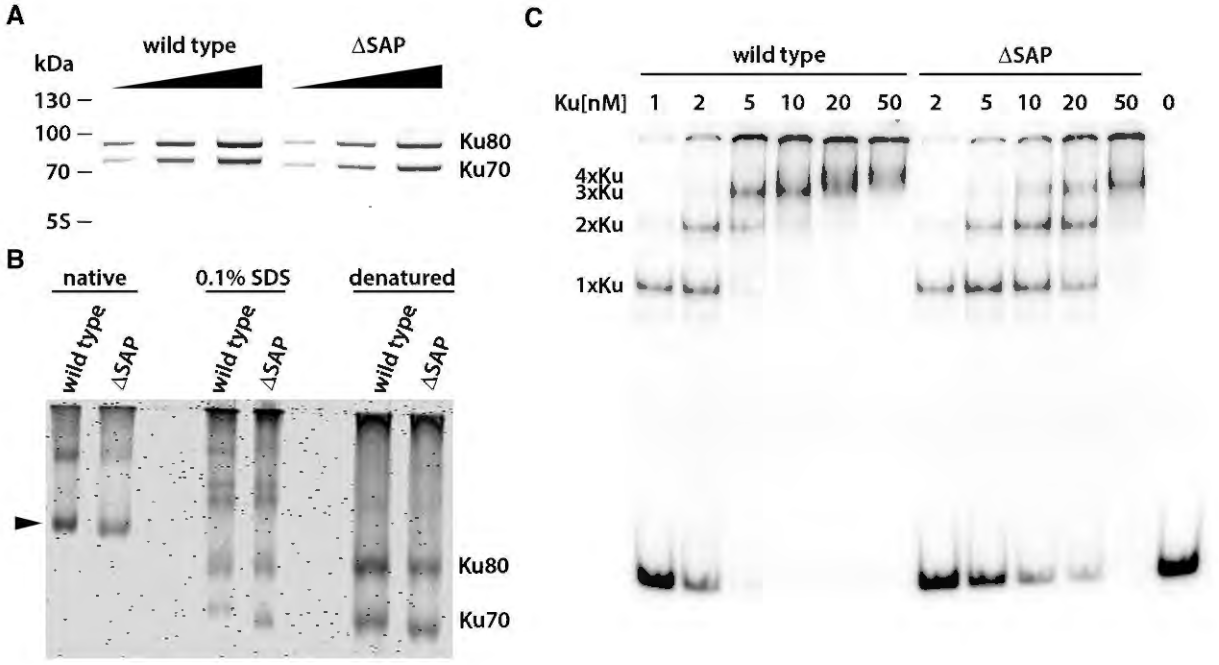

Figure 2. Biochemical characterization of the Ku ΔSAP complex. (**A**) SDS-PAGE of purified recombinant Ku complexes stained by SimplyBlue SafeStain. (**B**) Native-PAGE of recombinant Ku complexes demonstrates that deletion of SAP does not hinder dimerization. Arrowhead indicates Ku70/Ku80 heterodimer. (**C**) EMSA of a radioactively labeled 98-bp DNA probe (0.3 nM) with increasing concentrations of recombinant Ku complexes. Positions of Ku–DNA complexes with different stoichiometries are indicated on the left side of the gel.

data, together with telomere length analysis, indicates that despite its decreased DNA-end binding efficiency and lower expression in transgenic plants, Ku70 ΔSAP is fully proficient in telomere protection.

We next tested the proficiency of *ΔSAP* plants in DNA repair. Arabidopsis *ku70* and *ku80* mutants are highly sensitive to the radiomimetic drug bleomycin (12,37). The majority of seedlings of *ku70* mutants germinated on agar plates supplemented with a low concentration of bleomycin (50 ng/ml) either do not develop or have malformed true leaves, whereas wild type plants exhibit similar aberrations at three times higher concentrations (Figure 5A). This sensitivity is also apparent in the root growth assay, where root development in *ku70* mutants is completely arrested in agar plates supplemented with 25 ng/ml of bleomycin, whereas roots in wild type develop normally (Figure 5B). Intriguingly, *ΔSAP* plants behave similar to wild type in both seedling germination and root growth assays and do not exhibit increased sensitivity

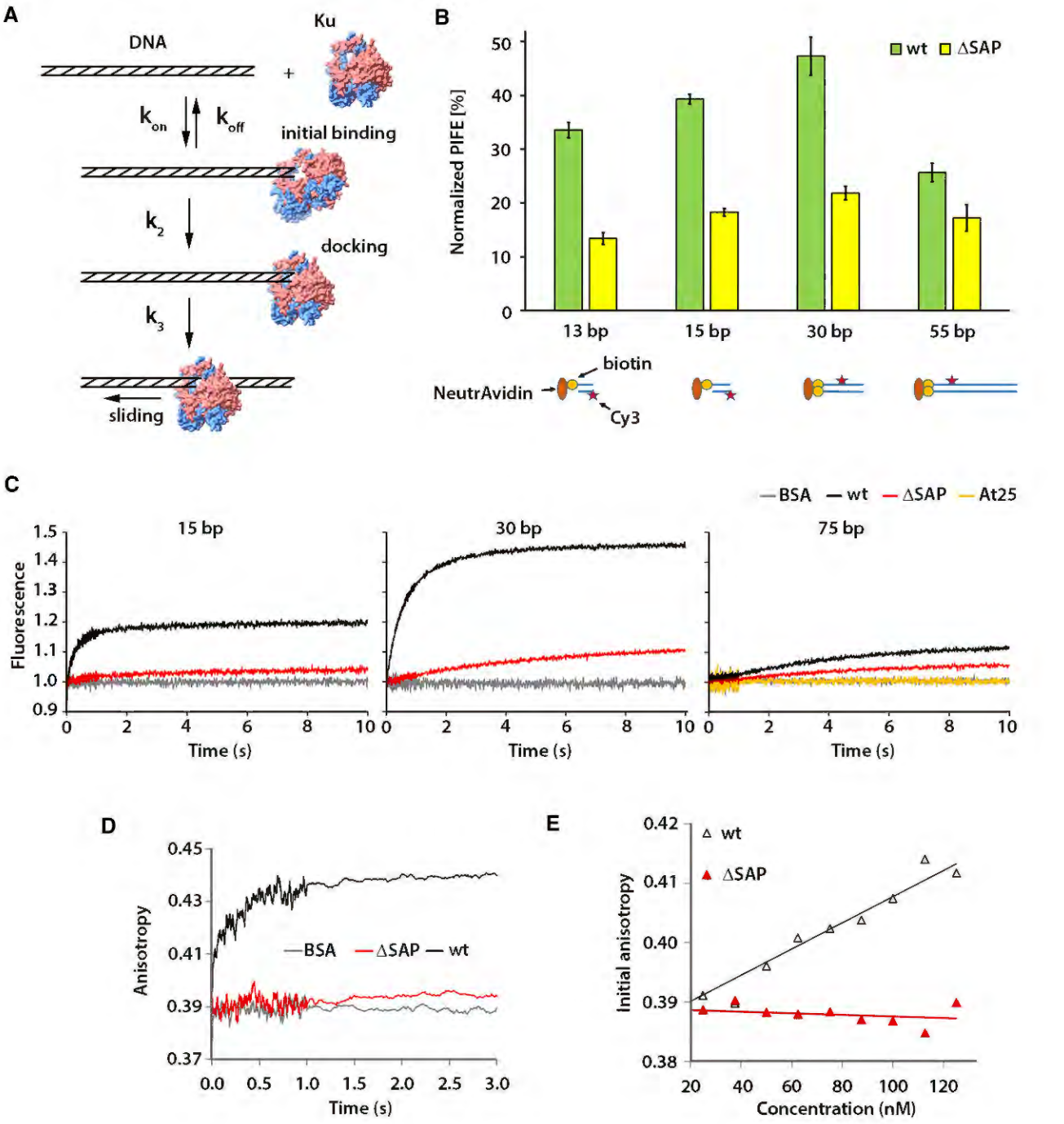

Figure 3. Mechanism of Ku DNA interaction. (**A**) Model of different phases of Ku DNA interaction. (**B**) Steady-state interaction of Ku at different positions along the DNA probe measured by mwPIFE. PIFE was calculated as the relative difference in fluorescence upon protein binding. Error bars represent standard deviations from two replicas. (**C**) Kinetic analysis of Ku–DNA binding by stopped-flow PIFE using the 15-, 30- and 75-bp DNA probes. Each trace represents the average of at least five individual measurements. The non-binding Ku variant (At25) was used as a control in the experiment with the 75 bp probe. (**D**) Anisotropy data from the stopped-flow measurements with the 30 bp probe. (**E**) Chart showing the dependence of the initial anisotropy (time point zero) on the concentration of the Ku complex.

to bleomycin (Figure 5, Supplementary Table S2). These data indicate that the Ku complex lacking the SAP domain is not substantially hindered in DNA repair.

NHEJ is the primary route of DSB repair in G0/G1 and is initiated by the binding of Ku to broken DNA ends, which limits excessive end resection. In the absence of Ku, DSBs can be repaired by alt-EJ, which can be distinguished by the production of larger deletions, typically more than 10 bp, at the site of repair (38,39). To evaluate whether the less efficient binding of Ku70 ΔSAP to DNA ends skews DSB repair towards alt-EJ, we designed an end joining assay based on the ligation of a linear DNA fragment transfected into plant protoplasts (Supplementary Figure S1). End joining products were PCR amplified 24 hr after transfection using primers spanning 225 bp of the ligation site, subjected to next generation sequencing, and the joined ends were analyzed to determine the

Table 1. Kinetic parameters for DNA interaction with wild type and ΔSAP

		Initial binding			Docking	Sliding
		k_{on} nM^{-1} s^{-1}	k_{off} s^{-1}	K_D nM	k_2 s^{-1}	k_3 s^{-1}
wt	15 bp	0.021 ± 0.005	2.0 ± 0.4	95	0.6 ± 0.1	–
ΔSAP	15 bp	0.002 ± 0.001	0.36 ± 0.09	180	0.2 ± 0.1	–
wt	30 bp	0.023 ± 0.005	1.4 ± 0.4	61	0.78 ± 0.07	–
ΔSAP	30 bp	0.002 ± 0.001	0.21 ± 0.12	105	0.09 ± 0.02	–
wt	75 bp	–	–	–	–	0.19 ± 0.05
ΔSAP	75 bp	–	–	–	–	0.14 ± 0.03

Kinetics analysis was performed with three different DNA substrates to identify the effect of the SAP domain on individual kinetic phases of Ku–DNA interaction. The 15 and 30 bp probes show the fast initial binding followed by a docking phase, 75 bp was used to monitor the kinetics of the sliding phase. The estimates for the rate constants of Ku–DNA association (k_{on}) and dissociation (k_{off}), docking (k_2) and sliding (k_3) phases were obtained by analytical fitting from the concentration dependence of the observed rates (Figure S2). The reported equilibrium dissociation constant was calculated from the rate constants ($K_D = k_{off}/k_{on}$).

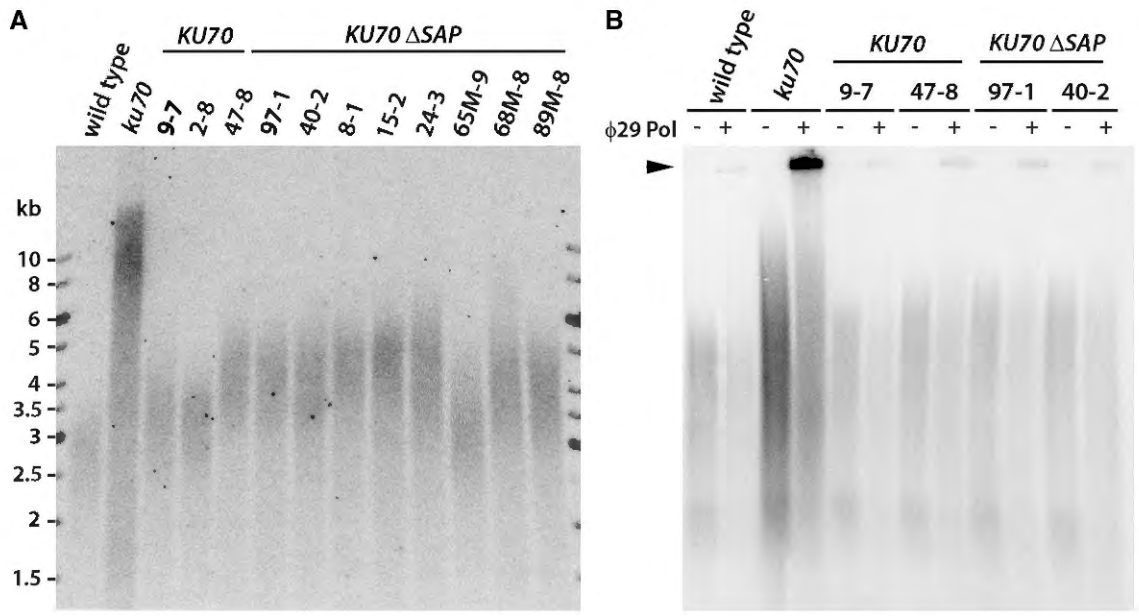

Figure 4. Effect of SAP on telomere maintenance. (**A**) Terminal restriction fragment length analysis with *Tru1*I-digested genomic DNA from wild type, *ku70* mutants and *ku70* mutants complemented either with wild type *KU70* or *ΔSAP KU70* constructs. Several independent complemented lines in T2 generation were analyzed. (**B**) The presence of t-circles detected by t-circle amplification assay. Reactions without phi29 polymerase were run in parallel as a control. The signal from t-circles is indicated by the arrowhead. Two independent lines were analyzed for each complementation construct.

extent of DNA resection prior to ligation. A large portion of joined ends exhibited deletions larger than 10 bp, even in Ku proficient protoplasts (Figure 6). We suspect that this reflects the rapid nucleolytic resection of naked chromatin-free DNA prior to its association with Ku, rather than a predominance of alt-EJ in Arabidopsis protoplasts. Nevertheless, the fraction of NHEJ events containing intact ends or deletions smaller than 10 bp was substantially larger in Ku-proficient cells compared to protoplasts from *ku70* mutants. We also included in the analysis protoplasts from At18 plants that contain a Ku complex that is hindered in sliding along DNA (12). We anticipated that the entrapment of Ku at DNA ends due to inefficient sliding would provide better end-protection and less resection. Indeed, the fraction of end-joining products with intact or less resected ends was greater in At18 than in plants with wild type Ku. *ΔSAP* protoplasts exhibited a similar end-resection pattern as Ku-proficient plants, suggesting that deletion of the SAP domain does not substantially compromise NHEJ.

Discussion

Ku plays a crucial role as an early responder to DNA damage by rapidly binding to DNA double-strand breaks (DSBs) and other free ends of DNA duplexes. The atomic structure of Ku provided crucial insight into the mechanism behind its sequence non-specific affinity for DNA ends (9). The Ku complex adopts a ring-like structure with a cradle at its base that allows DNA to thread through a preformed channel, thereby enabling Ku to load exclusively through DNA ends. The inner surface of the channel is composed of positively charged amino acid residues, which can potentially attract the negatively charged DNA backbone. Notably, the channel aperture appears smaller than the diameter of the duplex DNA, and its inner lining resembles a helical thread, suggesting that Ku may bind to DNA akin to a bolt on a nut.

Such a mode of interaction predicts that loading requires the precise positioning of a DNA end at the entry to the Ku channel and may represent the rate-limiting step. Our stopped-flow analysis indicates that Ku–DNA binding occurs

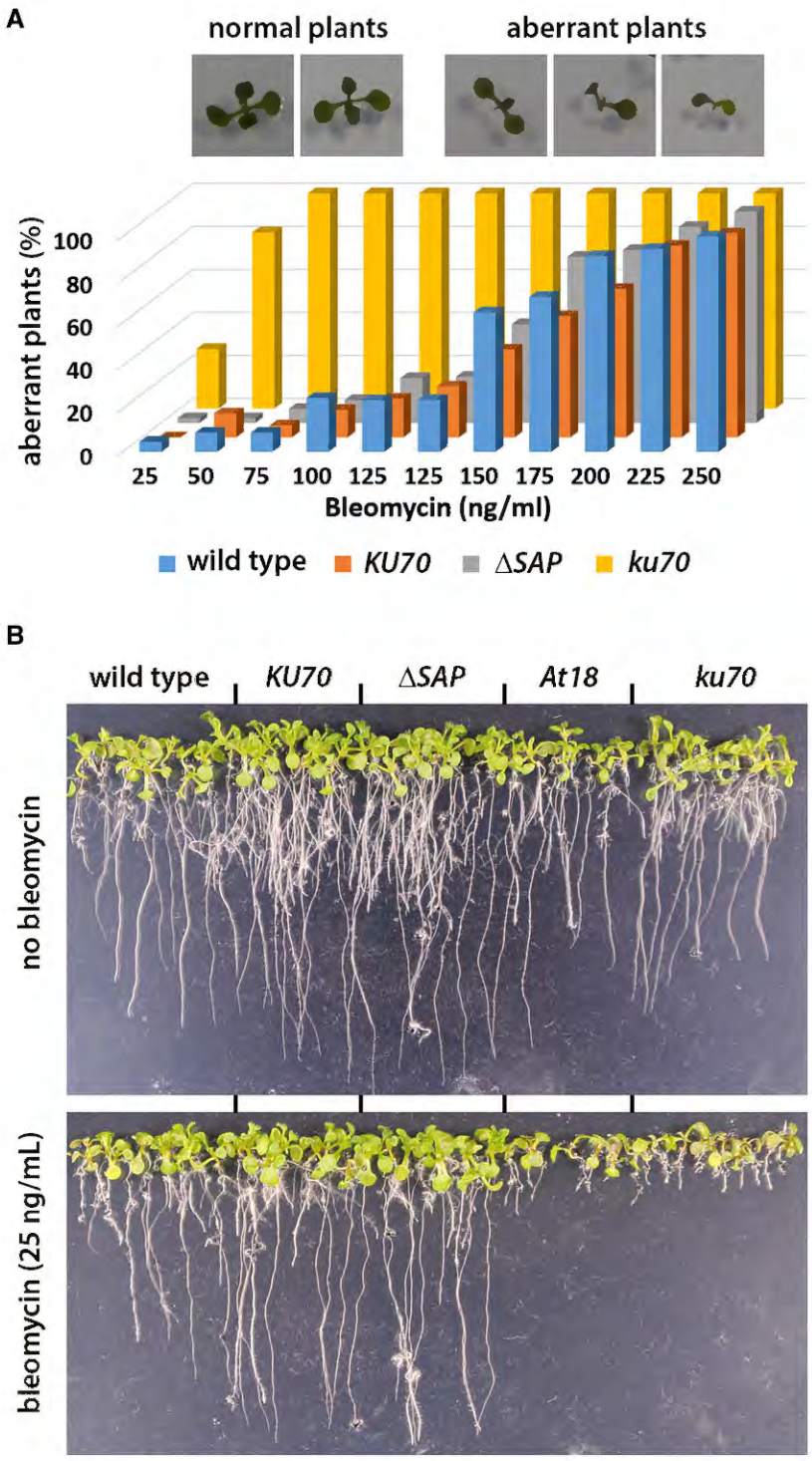

Figure 5. Sensitivity to bleomycin. (**A**) Seedling growth assay. Pictures show normally developed and sick seedlings with malformed true leaves 11 days after germination on media supplemented with bleomycin. 3D column chart indicates frequency of normal and sick seedlings germinated on media with different concentrations of bleomycin. At least 50 seedlings were count for each category of plants that included wild type, *ku70* mutants and *ku70* mutants complemented with either wild type, *ΔSAP* or *At18 KU70* constructs. *P*-values showing significance of the difference between the genotypes are presented in Table S2. (**B**) Root growth on media with or without bleomycin 11 days after germination.

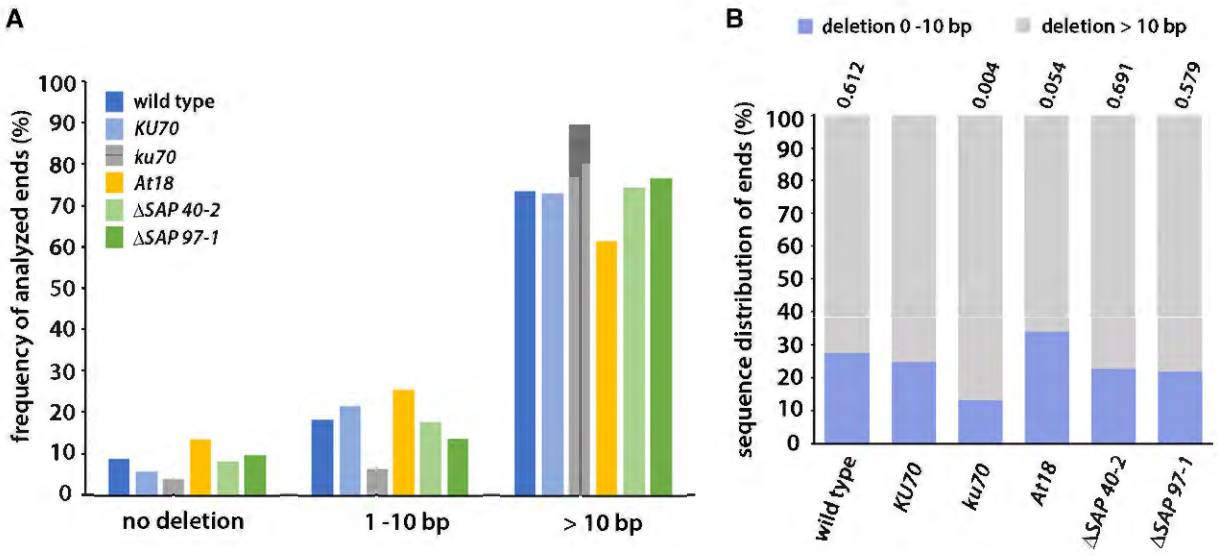

Figure 6. Sequence analysis of fusion junctions in the end-joining assay. (**A**) Frequency of DNA ends with different degree of resection scored in the end joining assay. The extent of the resection was calculated from the point of cleavage. Each ligated product provided information on two DNA ends. 73000 to 122000 amplicons were scored in each category that included wild type, *ku70* mutants, and *ku70* mutants complemented with either wild type, *ΔSAP* (two independent lines), or *At18 KU70* constructs. (**B**) Proportion of DNA ends with deletions larger than 10 bp in amplicons of different sequences. Frequency of each unique amplicon is not considered in the analysis. 85–104 most abundant types of amplicons unique in their sequence were scored in each category. *P*-values indicating significance of the difference from mutant complemented with the wild type construct (*KU70*) are indicated above each frequency bar (Yate´s chi-squared test).

in two kinetic phases, which we interpret as rapid initial contacts between Ku and DNA, followed by a slower step that may represent the docking of Ku onto DNA, analogous to positioning a nut onto a bolt (Figure 3A) (12). Once Ku is loaded, it can freely slide along DNA. The positioning of the DNA end is likely driven by electrostatic interactions with positively charged amino acids in the entry of the channel and the cradle facing the DNA. This is supported by observations that mutations reverting the charge at these positions abolishes Ku–DNA binding (11,12).

Studies on human Ku (16,40) together with our data in Arabidopsis indicate an evolutionarily conserved role for the Ku70 SAP domain in DNA binding. Our work indicates that the SAP domain is involved in the initial steps of the Ku–DNA interaction. Kinetic analysis showed that the ΔSAP Ku-complex is impaired already in the first binding phase, suggesting its function in mediating first contacts with DNA or in stabilizing these initial interactions. Structure-based modeling predicted that positively charged patches on the surface of the SAP domain and the flexible linker may interact with DNA (16,17). Thus, the Ku70 C-terminus may act as an extended flexible holder that can grab a free DNA end and drag it to the channel, or stabilize the initial interactions during loading of Ku onto DNA. This is further supported by the observation that the ΔSAP variant of human Ku very rapidly dissociates from a DNA substrate in a FRET-based assay (40). This model is also consistent with a recent structural analysis of human Ku showing that, in the DNA-free conformation, SAP is located at the leading face of the complex in the vicinity of the channel (18). This may also contribute to the directionality of the Ku–DNA binding.

The SAP domain could also potentially play a role in later steps of the Ku–DNA interaction. For example, it could assist in Ku translocation along DNA by diffusion-ratchet mechanisms (41), or stabilize established interactions by preventing Ku from sliding off the DNA. However, we did not observe an impact of SAP on the kinetics of Ku translocation along DNA, and the SAP domain appears to be positioned away from DNA once Ku is stably bound (18). Additionally, the SAP domain does not affect Ku retention on DNA when it is in complex with DNA-PKcs, which displaces Ku from the DNA end to more internal positions (40,42). This supports the notion that the SAP domain is required during the initial binding, but is dispensable for the stable Ku–DNA interaction of the fully loaded complex.

Curiously, despite reduced efficiency of DNA binding and lower expression, ΔSAP Ku appears to be proficient in telomere maintenance and NHEJ in Arabidopsis. In NHEJ, Ku binding to a DSB prevents excessive nucleolytic resection and coordinates processing activities to form ligatable ends. In the absence of Ku, DNA ends are exposed to DNA resection, which can reveal microhomologies between complementary strands on the opposite sites of a DSB. These sequence microhomologies are utilized by alt-EJ pathways to facilitate synapsis and ligation of broken DNA ends (3). Ku-deficient Arabidopsis plants exhibit sensitivity to bleomycin (12,37), and sequence analysis of EJ- junctions, generated either by re-ligation of CRISPR/Cas9 induced breaks or chromosome end-to-end fusions, revealed larger deletions and more frequent microhomologies typical for alt-EJ (39,43).

We found that ΔSAP Ku fully rescues the bleomycin sensitivity of *ku70* mutants. Furthermore, end-joining assays performed by transfecting naked linear DNA into mesophyll protoplasts combined with high-throughput sequencing of fusion junctions showed a re-ligation pattern similar to wild type rather than to *ku70* mutants in terms of the frequency of larger (>10 bp) deletions. This indicates that even the less efficient loading of ΔSAP Ku onto DSBs is still sufficient to support NHEJ and prevent access of competing nucleases. This corroborates the observation that Ku70 constructs lacking the

SAP domain were able to restore V(D)J recombination and resistance to ionizing radiation in mouse cells (40,44). The SAP domain appears to be dispensable also at telomeres. In Arabidopsis, Ku protects telomeres through their physical sequestration within the binding channel (12,24). This prevents the resection of chromosome ends replicated by the leading strand mechanism, resulting in blunt-ended telomeres. In the absence of Ku, telomeres are resected by EXO1 and other nucleases, exposing long 3´overhangs that serve as substrates for homologous recombination or extension by telomerase (24–26). Efficient protection of telomeres from excessive elongation by telomerase and homologous recombination in ΔSAP plants argues that, like in the context of DSBs, the speed of Ku loading onto telomeres is not the decisive factor for outcompeting these other end processing activities.

Data availability

The data underlying this article are available in the article and in its online supplementary material.

Supplementary data

Supplementary Data are available at NAR Online.

Acknowledgements

The project was supported by the Czech Science Foundation (19–21961S) to J.F. Scientific data presented in this paper were obtained with the support of the following Core Facilities (CF) of CEITEC Masaryk University: Plant Science CF, CF Bioinformatics, Genomics CF (supported by MEYS CR infrastructure project LM2023067) and CELLIM (supported by MEYS CR infrastructure project LM2023050 Czech-BioImaging). Z.P. was supported by the European Union's Horizon 2020 research and Innovation program TEAMING 857560, the Czech Ministry of Education, Youth and Sports TEAMING CZ.02.1.01/0.0/0.0/17_043/0009632), ESFRI RECETOX RI (LM2023069) and EXCELES Onco LX22NPO5102.

Funding

Czech Ministry of Education, Youth and Sports [CZ.02.1.01/0.0/0.0/17_043/0009632, LM2023069, LX22NPO5102]; Grantová Agentura České Republiky [19-21961S]; HORIZON EUROPE European Innovation Council [TEAMING 857560]; MEYS [LM2023042, LM2023067]. Funding for open access charge: Masaryk University.

Conflict of interest statement

None declared.

References

1. Mari,P.O., Florea,B.I., Persengiev,S.P., Verkaik,N.S., Bruggenwirth,H.T., Modesti,M., Giglia-Mari,G., Bezstarosti,K., Demmers,J.A., Luider,T.M., *et al.* (2006) Dynamic assembly of end-joining complexes requires interaction between Ku70/80 and XRCC4. *Proc. Nat. Acad. Sci. U.S.A.*, **103**, 18597–18602.
2. Koike,M., Yutoku,Y. and Koike,A. (2011) Accumulation of Ku70 at DNA double-strand breaks in living epithelial cells. *Exp. Cell. Res.*, **317**, 2429–2437.
3. Chang,H.H.Y., Pannunzio,N.R., Adachi,N. and Lieber,M.R. (2017) Non-homologous DNA end joining and alternative pathways to double-strand break repair. *Nat. Rev. Mol. Cell Biol.*, **18**, 495–506.
4. Sui,H., Hao,M., Chang,W. and Imamichi,T. (2021) The Role of Ku70 as a Cytosolic DNA Sensor in Innate Immunity and Beyond. *Front. Cell. Infect. Microbiol.*, **11**, 761983.
5. Balestrini,A., Ristic,D., Dionne,I., Liu,X.Z., Wyman,C., Wellinger,R.J. and Petrini,J.H. (2013) The Ku heterodimer and the metabolism of single-ended DNA double-strand breaks. *Cell Rep.*, **3**, 2033–2045.
6. Teixeira-Silva,A., Ait Saada,A., Hardy,J., Iraqui,I., Nocente,M.C., Freon,K. and Lambert,S.A.E. (2017) The end-joining factor Ku acts in the end-resection of double strand break-free arrested replication forks. *Nat. Commun.*, **8**, 1982.
7. Marcand,S. (2014) How do telomeres and NHEJ coexist?*Mol. Cell Oncol.*, **1**, e963438.
8. Zahid,S., Seif El Dahan,M., Iehl,F., Fernandez-Varela,P., Le Du,M.H., Ropars,V. and Charbonnier,J.B. (2021) The multifaceted roles of Ku70/80. *Int. J. Mol. Sci.*, **22**, 4134.
9. Walker,J.R., Corpina,R.A. and Goldberg,J. (2001) Structure of the Ku heterodimer bound to DNA and its implications for double-strand break repair. *Nature*, **412**, 607–614.
10. Yoo,S. and Dynan,W.S. (1999) Geometry of a complex formed by double strand break repair proteins at a single DNA end: recruitment of DNA-PKcs induces inward translocation of Ku protein. *Nucleic Acids Res.*, **27**, 4679–4686.
11. Britton,S., Coates,J. and Jackson,S.P. (2013) A new method for high-resolution imaging of Ku foci to decipher mechanisms of DNA double-strand break repair. *J. Cell Biol.*, **202**, 579–595.
12. Valuchova,S., Fulnecek,J., Prokop,Z., Stolt-Bergner,P., Janouskova,E., Hofr,C. and Riha,K. (2017) Protection of Arabidopsis blunt-ended telomeres is mediated by a physical association with the Ku heterodimer. *Plant Cell*, **29**, 1533–1545.
13. Aravind,L. and Koonin,E.V. (2000) SAP - a putative DNA-binding motif involved in chromosomal organization. *Trends Biochem. Sci*, **25**, 112–114.
14. Zhang,Z., Zhu,L., Lin,D., Chen,F., Chen,D.J. and Chen,Y. (2001) The three-dimensional structure of the C-terminal DNA-binding domain of human Ku70. *J. Biol. Chem.*, **276**, 38231–38236.
15. Anisenko,A.N., Knyazhanskaya,E.S., Zatsepin,T.S. and Gottikh,M.B. (2017) Human Ku70 protein binds hairpin RNA and double stranded DNA through two different sites. *Biochimie*, **132**, 85–93.
16. Wang,J., Dong,X., Myung,K., Hendrickson,E.A. and Reeves,W.H. (1998) Identification of two domains of the p70 Ku protein mediating dimerization with p80 and DNA binding. *J. Biol. Chem.*, **273**, 842–848.
17. Hu,S., Pluth,J.M. and Cucinotta,F.A. (2012) Putative binding modes of Ku70-SAP domain with double strand DNA: a molecular modeling study. *J. Mol. Model.*, **18**, 2163–2174.
18. Hnizda,A., Tesina,P., Nguyen,T.B., Kukacka,Z., Kater,L., Chaplin,A.K., Beckmann,R., Ascher,D.B., Novak,P. and Blundell,T.L. (2021) SAP domain forms a flexible part of DNA aperture in Ku70/80. *FEBS J.*, **288**, 4382–4393.
19. Rivera-Calzada,A., Spagnolo,L., Pearl,L.H. and Llorca,O. (2007) Structural model of full-length human Ku70-Ku80 heterodimer and its recognition of DNA and DNA-PKcs. *EMBO Rep.*, **8**, 56–62.
20. Khan,H. and Ochi,T. (2023) Plant PAXX has an XLF-like function and stimulates DNA end-joining by the Ku–DNA ligase IV-XRCC4 complex. *Plant J.*, **116**, 58–68.
21. Bundock,P., van Attikum,H. and Hooykaas,P. (2002) Increased telomere length and hypersensitivity to DNA damaging agents in an Arabidopsis KU70 mutant. *Nucleic Acids Res.*, **30**, 3395–3400.
22. Gallego,M.E., Bleuyard,J.Y., Daoudal-Cotterell,S., Jallut,N. and White,C.I. (2003) Ku80 plays a role in non-homologous recombination but is not required for T-DNA integration in Arabidopsis. *Plant J.*, **35**, 557–565.

23. Riha,K., Watson,J.M., Parkey,J. and Shippen,D.E. (2002) Telomere length deregulation and enhanced sensitivity to genotoxic stress in Arabidopsis mutants deficient in Ku70. *EMBO J.*, **21**, 2819–2826.
24. Kazda,A., Zellinger,B., Rossler,M., Derboven,E., Kusenda,B. and Riha,K. (2012) Chromosome end protection by blunt-ended telomeres. *Genes Dev.*, **26**, 1703–1713.
25. Riha,K. and Shippen,D.E. (2003) Ku is required for telomeric C-rich strand maintenance but not for end-to-end chromosome fusions in Arabidopsis. *Proc. Nat. Acad. Sci. U.S.A.*, **100**, 611–615.
26. Zellinger,B., Akimcheva,S., Puizina,J., Schirato,M. and Riha,K. (2007) Ku suppresses formation of telomeric circles and alternative telomere lengthening in Arabidopsis. *Mol. Cell*, **27**, 163–169.
27. Stoynova,L., Solorzano,R. and Collins,E.D. (2004) Generation of large deletion mutants from plasmid DNA. *BioTechniques*, **36**, 402–404.
28. Fulnecek,J. and Riha,K. (2021) High-throughput protein-nucleic acid interaction assay based on protein-induced fluorescence enhancement. *Methods Mol. Biol.*, **2209**, 109–117.
29. Johnson,K.A., Simpson,Z.B. and Blom,T. (2009) Global Kinetic Explorer: a new computer program for dynamic simulation and fitting of kinetic data. *Anal. Biochem.*, **387**, 20–29.
30. Yoo,S.D., Cho,Y.H. and Sheen,J. (2007) Arabidopsis mesophyll protoplasts: a versatile cell system for transient gene expression analysis. *Nat. Protoc.*, **2**, 1565–1572.
31. Zhang,J.J., Kobert,K., Flouri,T. and Stamatakis,A. (2014) PEAR: a fast and accurate Illumina Paired-End reAd mergeR. *Bioinformatics*, **30**, 614–620.
32. Dobin,A., Davis,C.A., Schlesinger,F., Drenkow,J., Zaleski,C., Jha,S., Batut,P., Chaisson,M. and Gingeras,T.R. (2013) STAR: ultrafast universal RNA-seq aligner. *Bioinformatics*, **29**, 15–21.
33. Robinson,J.T., Thorvaldsdottir,H., Winckler,W., Guttman,M., Lander,E.S., Getz,G. and Mesirov,J.P. (2011) Integrative genomics viewer. *Nat. Biotechnol.*, **29**, 24–26.
34. Senior,A.W., Evans,R., Jumper,J., Kirkpatrick,J., Sifre,L., Green,T., Qin,C., Zidek,A., Nelson,A.W.R., Bridgland,A., *et al.* (2020) Improved protein structure prediction using potentials from deep learning. *Nature*, **577**, 706–710.
35. Valuchova,S., Fulnecek,J., Petrov,A.P., Tripsianes,K. and Riha,K. (2016) A rapid method for detecting protein-nucleic acid interactions by protein induced fluorescence enhancement. *Sci. Rep.*, **6**, 39653.
36. Gallego,M.E., Jalut,N. and White,C.I. (2003) Telomerase dependence of telomere lengthening in Ku80 mutant Arabidopsis. *Plant Cell*, **15**, 782–789.
37. Fulcher,N. and Sablowski,R. (2009) Hypersensitivity to DNA damage in plant stem cell niches. *Proc. Nat. Acad. Sci. U.S.A.*, **106**, 20984–20988.
38. Hussain,S.S., Majumdar,R., Moore,G.M., Narang,H., Buechelmaier,E.S., Bazil,M.J., Ravindran,P.T., Leeman,J.E., Li,Y., Jalan,M., *et al.* (2021) Measuring nonhomologous end-joining, homologous recombination and alternative end-joining simultaneously at an endogenous locus in any transfectable human cell. *Nucleic Acids Res.*, **49**, e74.
39. Shen,H., Strunks,G.D., Klemann,B.J., Hooykaas,P.J. and de Pater,S. (2017) CRISPR/Cas9-induced double-strand break repair in Arabidopsis nonhomologous end-joining mutants. *G3*, **7**, 193–202.
40. Inagawa,T., Wennink,T., Lebbink,J.H.G., Keijzers,G., Florea,B.I., Verkaik,N.S. and van Gent,D.C. (2020) C-terminal extensions of Ku70 and Ku80 differentially influence DNA end binding properties. *Int. J. Mol. Sci.*, **21**, 6725.
41. Ait-Haddou,R. and Herzog,W. (2003) Brownian ratchet models of molecular motors. *Cell Biochem. Biophys.*, **38**, 191–214.
42. Chen,X., Xu,X., Chen,Y., Cheung,J.C., Wang,H., Jiang,J., de Val,N., Fox,T., Gellert,M. and Yang,W. (2021) Structure of an activated DNA-PK and its implications for NHEJ. *Mol. Cell*, **81**, 801–810.
43. Heacock,M., Spangler,E., Riha,K., Puizina,J. and Shippen,D.E. (2004) Molecular analysis of telomere fusions in Arabidopsis: multiple pathways for chromosome end-joining. *EMBO J.*, **23**, 2304–2313.
44. Jin,S. and Weaver,D.T. (1997) Double-strand break repair by Ku70 requires heterodimerization with Ku80 and DNA binding functions. *EMBO J.*, **16**, 6874–6885.
45. Pettersen,E.F., Goddard,T.D., Huang,C.C., Meng,E.C., Couch,G.S., Croll,T.I., Morris,J.H. and Ferrin,T.E. (2021) UCSF ChimeraX: structure visualization for researchers, educators, and developers. *Protein Sci.*, **30**, 70–82.

Received: June 26, 2023. **Revised:** September 11, 2023. **Editorial Decision:** September 14, 2023. **Accepted:** September 29, 2023